Multimaterial Fiber Microelectromechanical Systems Based on Electrostrictive P(VDF-TrFE-CFE)

By

Jefferson Clayton

B.A. Chemistry,
Princeton University, Princeton, NJ, 2011

Submitted to the Department of Materials Science and Engineering in partial fulfillment of the requirements for the degree of

Masters of Science in Materials Science and Engineering

at the

MASSACHUSETTS INSTITUTE OF TECHNOLOGY

September 2015

Author_____
Department of Materials Science and Engineering
August 13, 2015

Certified by_____
Yoel Fink
Professor of Materials Science
Professor of Electrical Engineering and Computer Science
Thesis Supervisor

Accepted by_____
Donald Sadoway
Chair, Departmental Committee on Graduate Students

Multimaterial Fiber Microelectromechanical Systems Based on Electrostrictive P(VDF-TrFE-CFE)

By

Jefferson Clayton

Submitted to the Department of Materials Science and Engineering on August 13, 2015, in partial fulfillment of the requirements for the degree of

Masters of Science in Materials Science and Engineering

Abstract

The miniaturization of electromechanical transducers using bulk and surface micromachining processes has enabled the deployment of microelectromechanical systems (MEMS) in a variety of applications, from cell phones and ink-jet printers to drug delivery devices. A recently developed approach for the fabrication of multimaterial fiber devices presents a unique opportunity to realize MEMS in a novel form. In this paper a thermally drawn MEMS fiber device based on P(VDF-TrFE-CFE) ferrorelaxor terpolymer is presented. Electromechanical actuation capabilities of this fiber device are established with a maximum strain of 0.78% and a maximum transverse deflection of 7μm under an applied voltage of 300VDC. The potential of this approach to realize complex electromechanical systems in fibers is illustrated by the fabrication of an electrostrictive device capable of modulating a light source reflected off the surface of the fiber. Amplitude modulation of incident light through electric field induced deflection is demonstrated up to the second harmonic frequency of the fiber at 158.3Hz, and a modulation depth of 22.5% is reported; for an array of such fibers in PDMS, amplitude modulation is demonstrated at low frequencies with a modulation depth of 25.8%. These results pave the way to the realization of sophisticated MEMS in fiber, with potential applications in large surface area devices such as interactive haptic displays, acoustic modulators, and energy harvesting systems.

Thesis Supervisor: Yoel Fink

Title: Professor of Materials Science and Engineering

Professor of Electrical Engineering and Computer Science

Acknowledgements

First and foremost, I would like to thank my thesis advisor, Dr. Yoel Fink, for his inspiration and guidance throughout my time spent at MIT. His advice and insights played critical roles in the research described in this thesis. I would also like to thank Dr. Noemie Chocat, who first taught me how to fabricate and characterize piezoelectric fibers. I would also like to thank Dr. Alexander Gumennik and Dr. Alexander Stolyarov, who taught me much of what I know about optics. I owe a sincere thank you to Dr. Etgar Levy, who not only assisted with challenging measurements but who also taught me how to be a better scientist. I would like to thank the rest of my labmates: Michael Rein, Benjamin Grena, Dr. Xiaoting Jia, Dr. Lei Wei, Chong Hou, and Rodger Yuan for being supportive and always willing to chat about new ideas or measurements. I reserve a special thank you for fellow labmate, Tara Sarathi, for being a great friend throughout grad school. Finally, I would like to thank my family and friends, as well as my fiancé, for supporting me through the tough times these past few years. I could not have done any of this alone.

Table of Contents

Table of Figures

Chapter 1

Introduction

Although the potential for miniature machines was appreciated as early as the 1960s, most famously in Richard Feynman's seminal lecture "There is plenty of room at the bottom" [1], the key enabler for the realization of microelectromechanical systems (MEMS) proved to be the vast knowledge on silicon material and processing technologies developed for the integrated circuit industry in the 1970s and 1980s [2]. Applying silicon micromachining technology to mechanical devices such as cantilevers and membranes, researchers have been able to fabricate increasingly sophisticated miniaturized electromechanical transducers. Today, MEMS have extended the applications of electromechanical transduction well beyond traditional actuation and motion sensing into new fields such as inkjet printing, accelerometers, drug delivery, and projection displays [3]. In the past decade, a new way of embedding devices in fibers has emerged, where fibers are not used as simple longitudinal conduits but as transverse devices that operate radially from their surface [4]. The thermal drawing process offers a scalable and controllable means of producing meters of uniform functional fiber with inner features of sub-micron dimensions. This approach has led to the successful development of optical, optoelectronic, electronic, and thermal fiber devices [4], and presents an opportunity to realize MEMS in a novel form. Just as their miniaturization allowed the deployment of MEMS for use in new applications, the realization of long, thin, and flexible fibers with electromechanical transduction capabilities would enable new sensing and actuating

applications in inaccessible regions or over extended lengths. The ability to assemble fiber devices into grids or fabrics lends them particularly well to the coverage of large non-planar surfaces [5,6] an important feature for applications such as energy harvesting or haptic displays. Furthermore, monolithic integration of electrodes into the fiber enables straightforward connection with external electrical circuits [7].

Recently, a thermally drawn piezoelectric device in fiber-form was demonstrated, achieving an important milestone in the development of MEMS in fibers [8]. Piezoelectric materials have found uses in multiple applications ranging from hydrophones to medical imaging, however typical piezoelectric strains on the order of ~0.1% fundamentally restrict the range of mechanical strain they can undergo and limit their usefulness as actuators. While electrostriction was long considered a higher-order nonlinear effect requiring stronger fields in most materials than typical fields used in piezoelectric materials, the emergence of a new class of highly electrostrictive materials, known as relaxor ferroelectrics, has opened the way for the use of electrostriction as an alternative to piezoelectricity for large-strain actuation applications.[9] In addition to strain capabilities of several percent, a major advantage of electrostriction over ferroelectric mechanisms is that it enables a reproducible, non-hysteretic response, with high temperature stability and absence of aging [9]. Furthermore, electrostrictors do not require high-field electrical poling, unlike ferroelectric piezoelectrics, and are more stable over time. Finally, electrostrictive materials can be used at high frequencies using their DC field-induced piezoelectric properties, and their electromechanical coefficients can be adjusted by changing the DC biasing field [10].

Here we report a novel thermally drawn MEMS fiber device based on P(VDF-TrFE-CFE) ferrorelaxor terpolymer. Electromechanical actuation capabilities of this fiber device are established using high voltage atomic force microscopy (HVAFM) and a strain of 0.78% is achieved. For a fiber with an asymmetric geometry with respect to placement of the electrostrictive layer, a maximum transverse deflection of 7μm under an applied voltage of 300VDC is established using contact profilometry. The potential of this approach to realize complex electromechanical systems in fibers is illustrated by the fabrication of an electrostrictive device capable of modulating a light source reflected off the surface of the fiber. Amplitude modulation of incident light through electric field induced deflection is demonstrated up to the second harmonic of the fiber at 158.3Hz, and a modulation depth of 22.5% is reported; for an array of such fibers in PDMS, amplitude modulation is demonstrated at low frequencies with a modulation depth of 25.8%.

This thesis is organized as follows. In Chapter 2, we lay the general framework for the fabrication of multimaterial function fibers as well as introduce background material on electrostriction. We discuss the thermal drawing process, materials selection criteria, and fabrication challenges. In Chapter 3, we present an in-fiber MEMS device based on electrostrostrictive P(VDF-TrFE-CFE). In Chapter 4, we predict fiber behavior using finite-element simulations, and then confirm the simulations by characterizing fiber strain and deflection. We demonstrate that our fiber is capable of controlled actuation. In Chapter 5, we utilize fiber actuation to perform amplitude modulation of an incident light source. We explore how modulation depth of the incident signal varies in the proximity of the first and second harmonic frequency of the fiber. We also demonstrate the potential for in-fiber MEMS to form

the basis of large-area devices by embedding an array of fibers in a polymer matrix and using the composite for light modulation. Finally, in Chapter 6, we conclude by outlining future research directions and applications.

Chapter 2

Background

2.1 Multimaterial Functional Fibers

Fiber fabrication through controlled heating and extrusion is a well-established process that played a key role in the development of the telecommunications industry and the widespread use of fiber optics. Until recently, the thermal drawing process was limited to silica, but over the past decade our research group has developed low-temperature methods for expanding the list of drawable materials to include polymer composites [5]. These techniques enable the rapid fabrication of kilometer-scale lengths of fiber with arbitrary cross-sections and unique functionalities. In this section, we cover the thermal drawing process and discuss how to select compatible materials when constructing fiber devices.

2.1.1 Fabrication Process

Fiber fabrication begins with an object known as a *preform*, which is identical in geometry and material composition to the final fiber, but is shorter in length and larger in cross-sectional dimensions. Typical dimensions for a preform are 1-5 cm in width and thickness and 20-30 cm

in length, while the fiber drawn from such a preform can be hundreds of microns in width and thickness and hundreds of meters in length (figure 1).

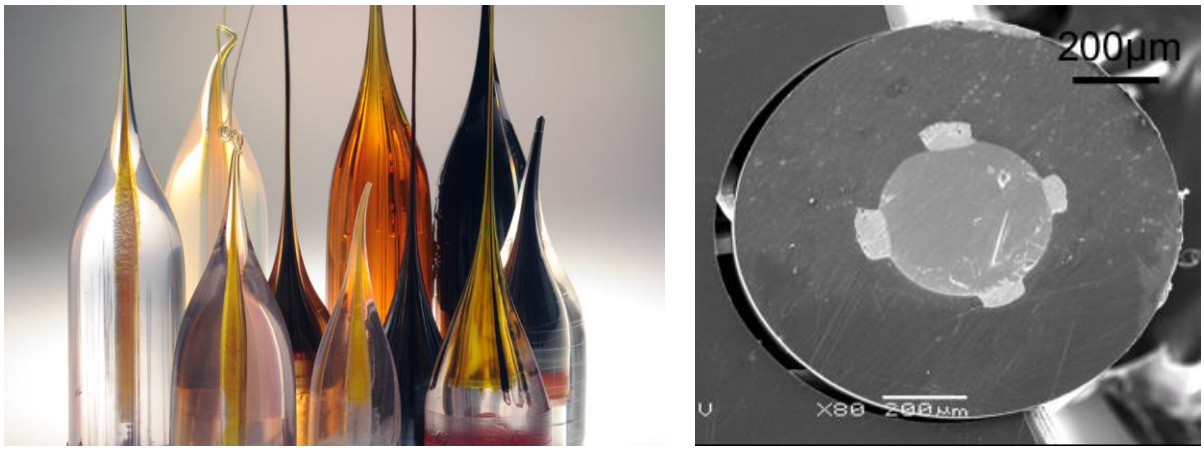

(a) (b)

Figure 1. a) Various post-draw preforms showing how the drawing process scales down cross-sectional dimensions (photo courtesy of Greg Hren). **b)** Cross-section of a fiber after the drawing process, showing features on the order of hundreds of microns (SEM micrograph courtesy of Fabien Sorin).

Depending on the desired geometry of the final fiber, preforms may be assembled using a variety of machining techniques such as milling, turning, evaporation, or rolling. Following assembly, the preform must then be consolidated in a vacuum oven at temperatures near the glass transition temperature of the cladding material in order to form high-quality interfaces and to evaporate trapped water vapor which can later form bubbles during the drawing process. The resulting consolidated preform is then ready to be drawn into a fiber using a draw tower (figure 2).

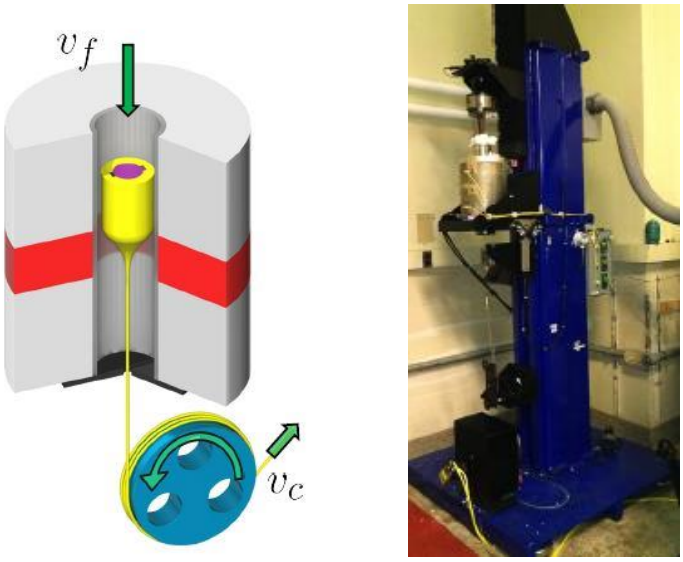

(a) (b)

Figure 2. a) Schematic of thermal drawing process (courtesy of Guillaume Lestoquy) **B)** low-temperature draw tower used for fiber fabrication.

At the fiber draw tower, the preform is fastened to a holder and then slowly lowered into a three-zone furnace, where it is heated in gradual ramps until it reaches a fluid state that is viscous enough to neck down under the effect of gravity. The neck-down region is fed into a capstan and pulled under continuous tension while maintaining internal and external geometry throughout the remainder of the draw. By conversation of volume, the draw-down ratio *r* is related to both the downfeed speed and capstan speed by:

$$r = \sqrt{\frac{v_{capstan}}{v_{downfeed}}} \quad (1)$$

Typical capstan speeds and downfeed speeds are on the order of ~m/min and ~mm/min, respectively, resulting in common draw-down ratios of 20-50. Fiber geometry and axial stress are continuously monitored throughout the draw using a combination of a laser micrometer and a tension meter, enabling informed adjustment of the draw parameters in real-time (figure 3).

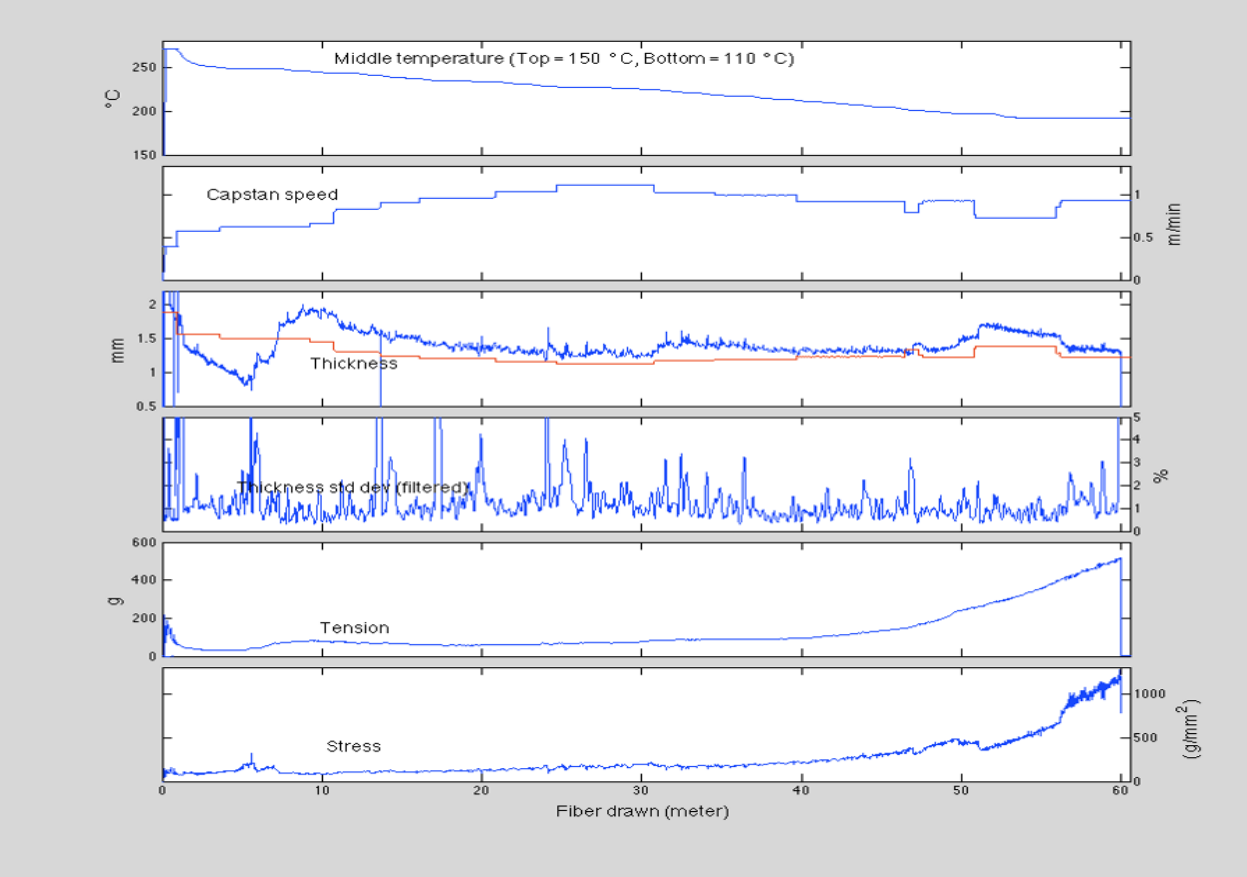

Figure 3. Example plots of draw parameters that can be monitored in real time, including furnace temperatures, capstan speed, fiber dimensions and standard deviation, and axial tension/stress.

2.1.2 Materials Selection Criteria

During the draw process, viscous forces are commonly used to oppose interface-energy-driven capillary break-up phenomena. A direct consequence of this is that not all materials can be drawn together, especially if their behaviors strongly vary at or near the draw temperature. To ensure maximum capability during the draw process, the following general conditions are followed for materials selection [4]:

1) At least one of the fiber materials must be able to support the draw stress while deforming in a continuous and controlled manner. Practically, this means that at least one component should be amorphous and resist devitrification, allowing for reasonable draw speeds while maintaining structural integrity.
2) All materials must flow at a common temperature, i.e. at the draw temperature their viscosities should be less than 10^7 Pa*s. Any crystalline material should have a melting temperature below the chosen draw temperature.
3) All materials should exhibit good adhesion and wetting in both the viscous and solid states, without cracking even when subjected to rapid cooling.

Owing to their excellent thermal and mechanical properties that fit within the draw criteria, high glass transition temperature thermoplastics are often employed as the cladding (bulk) material. Over the years, several thermoplastic polymers have been identified for draw temperatures between 200-300 C, and the fibers described in this thesis employ polycarbonate (PC) as a cladding material. Key to the introduction of new functionalities in fiber devices is then the identification of materials that both exhibit the desired behaviors and that can be co-drawn

with the cladding material. In the next section, we introduce how electromechanical transduction can be utilized to create in-fiber MEMS devices, and then select an appropriate material for our applications in the subsequent chapter.

2.2 Electromechanical Transduction Mechanisms

Electromechanical transduction mechanisms couple mechanical energy with electrical energy, and can be used to induce or sense strain in a material. Compared to other transduction mechanisms, their large bandwidth allows them to operate at frequencies ranging from Hz to GHz. They can also be electrically driven, which enables them to be easily integrated with driving electronics.

In differential form, the electromechanical properties of a solid can be described using the Gibbs function *G* as follows [11]:

$$\mathrm{d}G = -S\mathrm{d}T - \mathbf{x}_{ij}\mathrm{d}\mathbf{X}_{ij} + \mathbf{E}_i\mathrm{d}\mathbf{P}_i \quad (2)$$

where *G* is the free energy, *S* is the entropy, *T* is the temperature, **x** is the strain tensor, **X** is the stress tensor, **E** is the electric field, and **P** is the polarization. By differentiating *G* with respect to stress, one can obtain the tensor properties associated with strain-inducing effects in the material. At constant stress and temperature, the strain can be expressed as a power series of the polarization:

$$\mathbf{x}_{ij} = \mathrm{g}_{ijm}\mathbf{P}_m + \mathbf{Q}_{ijmn}\mathbf{P}_m\mathbf{P}_n + \cdots \quad (3)$$

with

$$\mathrm{g}_{ijm} = \left(\frac{\partial^2 G}{\partial \mathbf{X}_{ij} \partial \mathbf{P}_m} \right)_{\mathbf{X},T} \quad (4)$$

and

$$\mathbf{Q}_{ijmn} = \left(\frac{\partial^3 G}{\partial \mathbf{X}_{ij} \partial \mathbf{P}_m \partial \mathbf{P}_n} \right)_{\mathbf{X},T} \quad (5)$$

The linear coefficient g is related to the piezoelectric effect, while the quadratic coefficient Q is related to electrostriction. The mechanism employed in this thesis for in-fiber MEMS devices is electrostriction, which will be described in more detail in the following section.

2.2.1 Electrostriction

Electrostrictive strain is most generally described using the quadratic term from equation 3 above. The coefficients that compose the fourth-rank tensor Q are in units of m^4C^{-2} and are on the order of 10^{-3} m^4C^{-2} in relaxor ferroelectrics. Unlike piezoelectricity, which is only present in non-centrosymmetric materials, electrostriction is a property of all dielectric materials and does not requiring a poling step to induce desired behavior. When the material under study is subject to an electric field, the cations and anions are displaced in opposite directions and are attracted to each other, resulting in a contraction in the direction of the applied electric field. The reverse effect of expansion is impossible in electrostrictive materials, and reversing the direction of the electric field does not affect the sign or magnitude of the induced strain. A

direct consequence worth noting then is that electrostriction occurs at double the frequency of the applied field. Other advantages over piezoelectrics are a non-hysteretic response with high temperature stability and the absence of aging [9].

Electrostriction was long considered a higher-order, non-linear effect requiring excessively strong fields that made it an impractical effect to employ for actuation. This changed with the emergence of a new class of highly electrostrictive materials, known as relaxor ferroelectrics, which made electrostriction a viable alternative to piezoelectricity for large-strain applications [9]. The study of relaxor ferroelectrics originated from work on perovskite structure electroceramics and has experienced an explosive growth of interest with the discovery of large, stable electrostrictive strains in lead magnesium niobate (PMN) [12]. Electostrictive materials are now used in active optical systems, stacked actuators, artificial muscles, and energy-harvesting devices [10].

Chapter 3

Electrostrictive Fiber Fabrication

In this chapter, we introduce the fiber geometries and materials of interest for constructing in-fiber MEMS devices based on electrostriction. Draw process parameters are discussed, and the structural integrity of the post-draw fiber cross-section is investigated on an SEM.

3.1 Materials Selection

Recently, relaxor ferroelectric behavior was discovered in a thermoplastic compatible with the thermal drawing process, poly(vinylidene fluoride trifluoroethylene) (P(VDF-TrFE)), with electrostrictive strains of more than 7% for applied electric fields of 160MV/m [12]. The theoretical value for the electric field required to achieve the same strain in piezoelectric polymers would be above 2000MV/m, a value well beyond the dielectric breakdown strengths of these materials. The large strains achievable in ferrorelaxor P(VDF-TrFE) are a result of molecular orientational changes from the all-trans ferroelectric phase to the paraelectric phase, which has a mixture of trans and gauche conformations. In regular P(VDF-TrFE), this first-order phase transition occurs at temperatures above 100°C and is accompanied by a large hysteresis, which limits its practical use. By introducing defects into the polymer chains, it is possible to break the long-range polar regions into microdomains, which results in a broadening of the

ferroelectric transition. This can be achieved by electron irradiation or by introducing a small amount of ternary monomer with bulky groups such as chlorotrifluoroethylene (CTFE) and 1,1-chlorofluoroethylene (CFE) [13,14]. The resultant modified P(VDF-TrFE) polymers are ferrorelaxors, which exhibit large electromechanical strains at room temperature with minimal hysteresis. The advantage of the terpolymer approach is that it simplifies the process, since the resultant terpolymer is inherently electrostrictive without the need for any additional step such as irradiation. Furthermore, it removes undesirable side effects caused by irradiation, such as the formation of radicals, chain scission, and cross-linking. Of all the P(VDF-TrFE)-based terpolymers, P(VDF-TrFE-CFE) has been shown to exhibit the largest electromechanical strain and its use has been explored for various electromechanical applications [15], including applications found in this thesis.

3.2 Fiber Assembly and Fabrication Results

Previous work has demonstrated that ferroelectric P(VDF-TrFE) can be thermally drawn in a polycarbonate (PC) cladding with carbon-loaded polyethylene (CPE) electrodes [6]. Given that P(VDF-TrFE-CFE) has a melting temperature that is 25° lower than that of P(VDF-TrFE), it can be co-drawn with the same materials system. The P(VDF-TrFE-CFE) terpolymer was purchased in powder form and melt-pressed at 155°C under 110 bars to form 300 µm-thick films. It was then assembled into a preform with 300 µm-thick CPE films, eutectic $Bi_{58}Sn_{42}$ electrodes (T_M = 138°C), and PC bar cladding using traditional milling techniques (figure 4). The preform was

consolidated in a vacuum oven at 185°C for 20 minutes to remove trapped gas and form high quality interfaces. This final preform was 38 mm wide, 11 mm thick, and 200 mm long. It was then thermally drawn in a three-zone vertical tube furnace with the top-zone temperature at 150°C, the middle-zone temperature at 230°C, and the bottom-zone temperature at 110°C. The preform was fed into the furnace at a speed of 1 mm/min, and the fiber was drawn at a speed of 0.8 to 2.0 m/s. The tension during the draw was 100-200 g, corresponding to an average stress of 2-4 kPa. With this procedure, meters of fibers were drawn with thicknesses ranging from 230 to 370 µm (widths ranged from 800 µm to 1.3 mm).

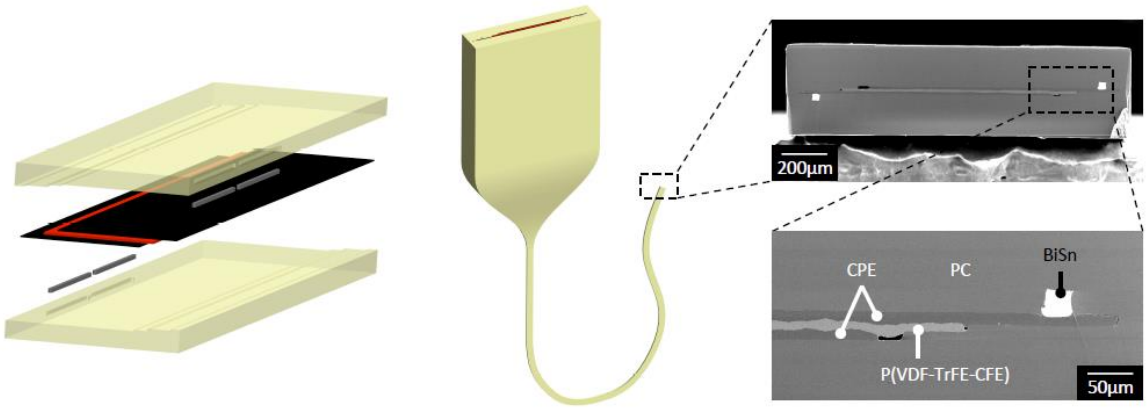

(a) (b) (c)

Figure 4. a) Schematic of the preform assembly for a multimaterial electrostrictive fiber. A P(VDF-TrFE-CFE) layer (red) is assembled with CPE polymer electrodes (black), Bi-Sn electrodes (grey), and a PC cladding (beige). **b)** Schematic of the preform-to-fiber draw process. **c)** SEM micrographs of the overall structure and close-up of a multimaterial electrostrictive fiber.

SEM micrographs of the cross-section of a multimaterial electrostrictive fiber show that the device structure is well conserved during the draw (figure 4). The materials show good adhesion and the sharp angles in the device architecture are maintained. Taking advantage of

the great freedom allowed by the thermal drawing method in the device materials and geometry, we also construct a hybrid fiber containing a chalcogenide glass mirror and an off-center electrostrictive device based on P(VDF-TrFE-CFE). The preform was prepared by milling a rectangular PC slab so as to smooth its edges and obtain a rounded rectangular cross-section. The resulting slab was assembled with 300 µm-thick CPE films, 300 µm-thick P(VDF-TrFE-CFE) layers, eutectic $Bi_{58}Sn_{42}$ electrodes, and a 300 µm-thick PC layer on top. $As_{25}S_{75}$ chalcogenide glass was synthesized in a rocking furnace using the melt-quench technique and evaporated onto 10 µm-thick PC films using a rotating drum evaporator to obtain uniform glass/polymer layers. The PC/glass bilayer film was then rolled around the preform. The preform was then consolidated in a vacuum oven for 20 minutes at 185 C, and drawn at 230 C (figure 5).

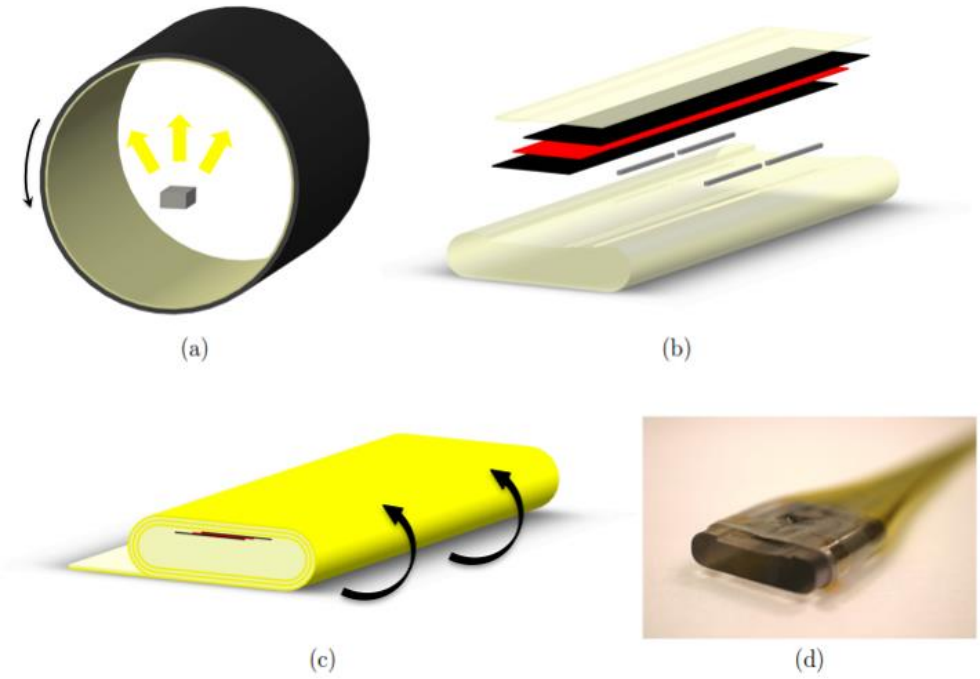

Figure 5. a) Schematic of rotating chamber using to evaporate chalcogenide glass onto PC films. **b)** Schematic of preform assembly method. **c)** Schematic of chalcogenide glass on PC film rolled around the assembled preform. **d)** Post-draw preform showing fiber necking.

SEM micrographs of the cross-section of an electrostrictive fiber with rolled chalcogenide glass mirror show that the device structure is well conserved during the draw (figure 6). The materials again show good adhesion and the sharp angles in the device architecture are maintained.

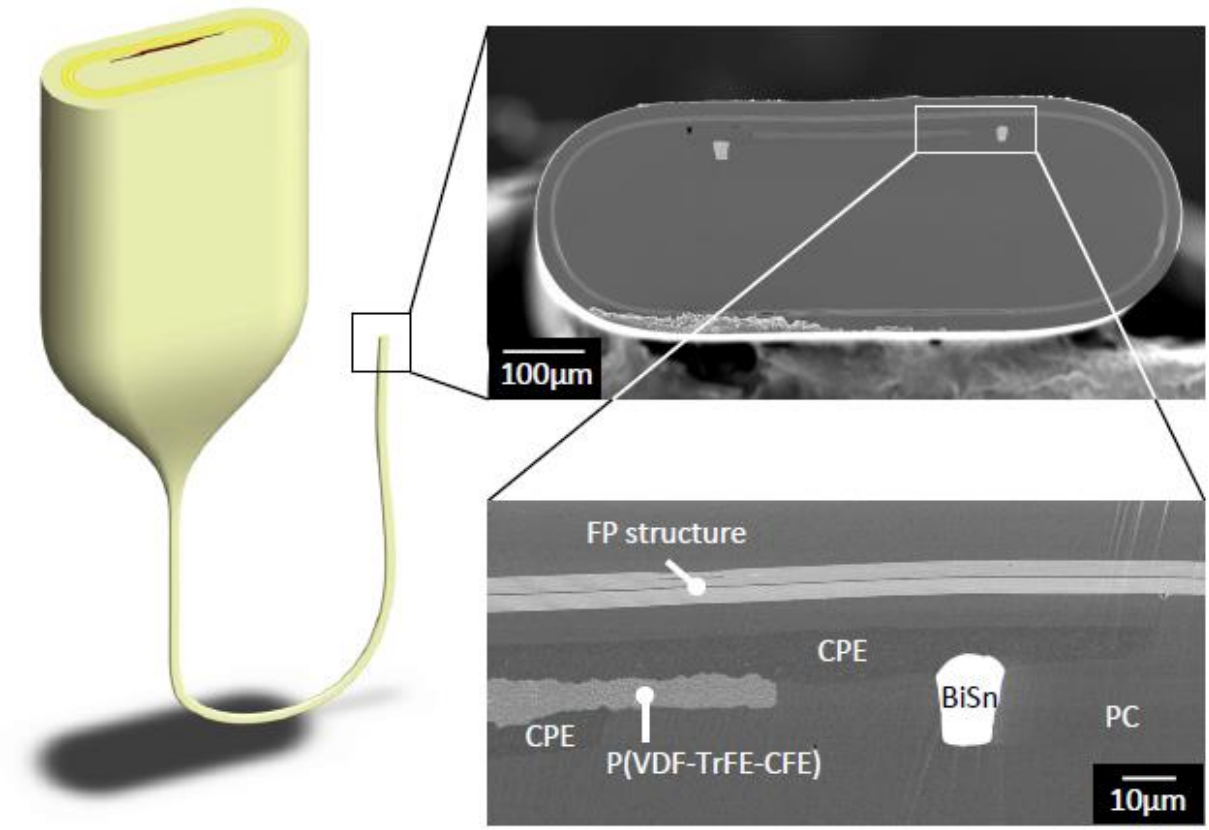

Figure 6. Thermal drawing process for fiber containing chalcogenide glass mirror and SEM micrographs of the post-draw cross-section. In this particular case, the fiber has been wrapped to create a Fabry-Perot optical cavity on the surface.

Figure 7 shows a close-up of the fibers after the thermal drawing process, as well as a collection of ~1m long fibers showing the many meters that can be obtained.

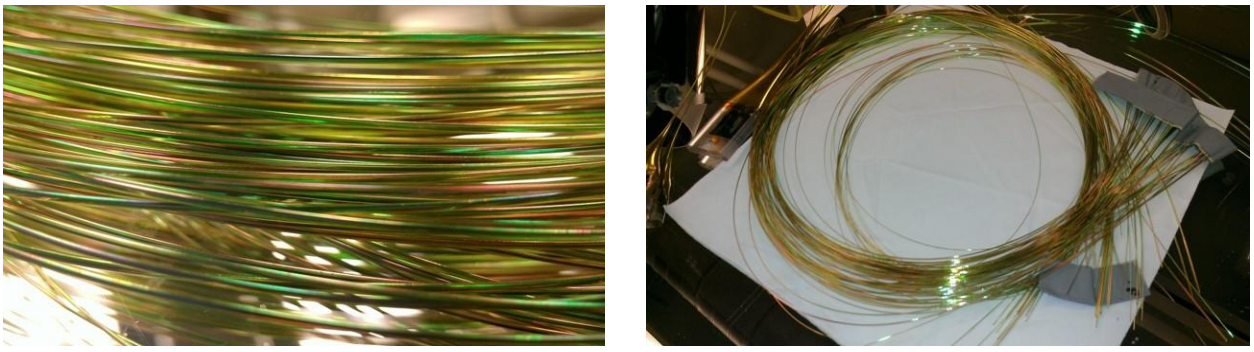

(a) (b)

Figure 7. a) Close-up of fibers containing a chalcogenide glass mirror. **b)** Photograph of the many meters of fibers that can be obtained during a single thermal drawing process.

It is worth pointing out that during the chalcogenide glass wrapping process, if the PC/glass film is wrapped many times around the preform, and then halfway through the preform is flipped so that the central PC layer would have double the thickness of the other PC layers, then a Fabry-Perot cavity can be formed on the fiber surface. Throughout the remainder of this thesis, this is the fiber structure that is utilized for actuation; however, the Fabry-Perot cavity is used simply as a mirror and requires further exploration. A reflective coating on the fiber, whether an integrated chalcogenide glass mirror or gold sputtered directly onto PC, helps increase the signal-to-noise ratio of measurements taken on light reflected off the surface of the fiber.

Chapter 4

Simulated and Measured Behavior

In this chapter, we study a thermally drawn fiber containing an off-center MEMS device based on electrostrictive P(VDF-TrFE-CFE). We first simulate the strain field in the surrounding PC cladding that would be induced by applying a uniform electric field across the electrostrictive layer. Predicted strain values are confirmed using high-voltage atomic force microscopy, and resulting micron-scale transverse deflection is observed using contact profilometry. This field-induced actuation, which resembles transverse deflection of a cantilever when one end of the fiber is clamped, will allow us to use these fibers to perform amplitude modulation of an incident light source in the next chapter.

4.1 Finite-Element Simulations

When a voltage is applied across the CPE electrodes of the fiber shown in Figure 5, the P(VDF-TrFE-CFE) layer contracts in the thickness direction and expands in the lateral direction (figure 8). This lateral strain should result in the creation of a strain field in the surrounding polycarbonate cladding. To verify this, simulations of the electric-field induced strain

distribution in the fiber structure are performed using a finite element software package, COMSOL. The results show a complex deformation of the fiber structure.

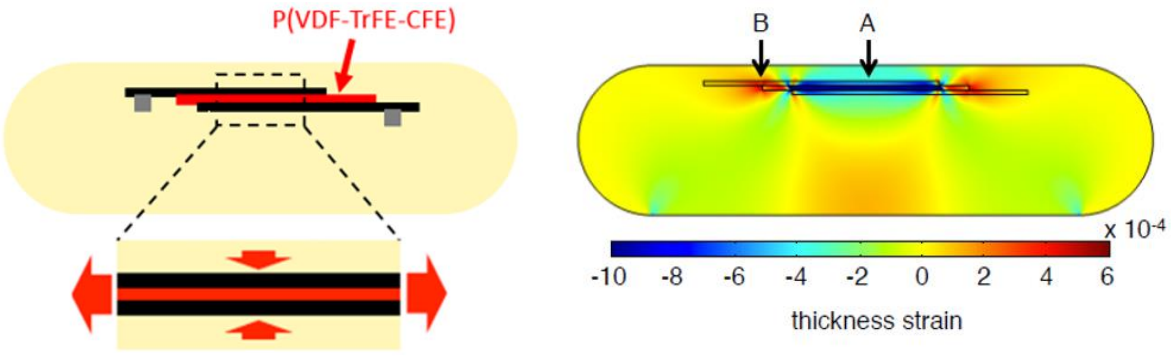

(a) (b)

Figure 8. a) Schematic of the principle of operation of the fiber, where electric field induced strain in the electrostrictive layer strains the surrounding PC cladding. **b)** Simulation of the electric field induced thickness strain distribution in the fiber under an applied voltage of 300V.

The central portion of the fiber behaves as expected, with a contraction of the electrostrictive layer resulting in a negative strain in the regions above and below it. However, this thickness contraction produces a lateral expansion of the electrostrictive layer due to the Poisson effect, which results in a positive strain in the lateral portions on either side of the terpolymer layer and in the central portion on the opposite face. This leads to an inhomogeneous strain field in the surrounding polycarbonate cladding, with both negative and positive strain regions that suggest a capability for transverse deflection. The finite element simulations show that the thickness strains corresponding to an electrostrictive layer contraction of 0.5% are on the order of $1\text{-}4.10^{-4}$.

4.2 High-Voltage Atomic Force Microscopy

The amount of electrostrictive strain achievable in these fibers was measured using a technique based on high voltage atomic force microscopy (HVAFM). Compared to traditional techniques where the voltage is applied via the AFM tip, HVAFM has the advantage of enabling higher and more uniform applied electric fields, and its use has been demonstrated for piezoelectric coefficient measurements [16]. Photographs of the experimental setup are shown in Figure 9, and a schematic of the setup is shown in Figure 10.

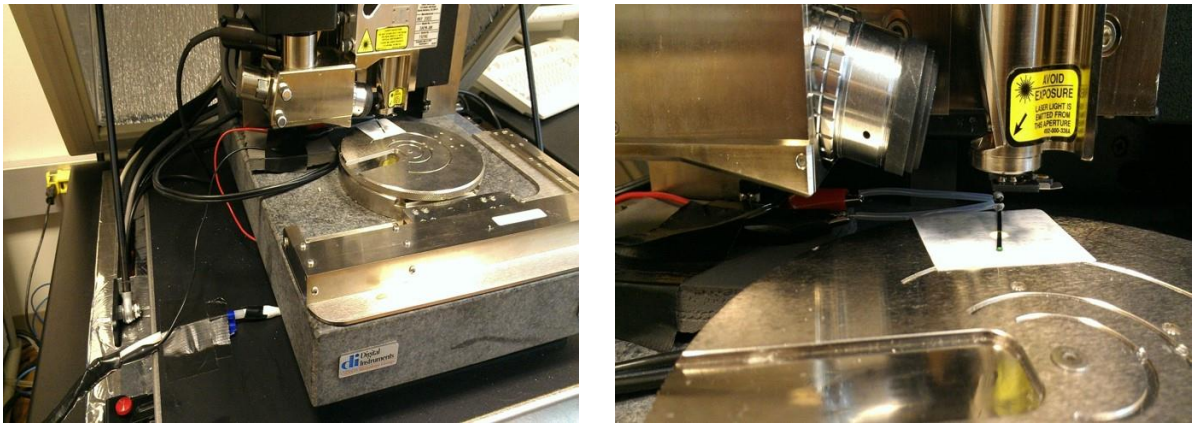

(a) (b)

Figure 9. a) Photograph of a fiber sample resting on an AFM stage, with electrical leads connected to a high-voltage power supply. **b)** Close-up of same fiber.

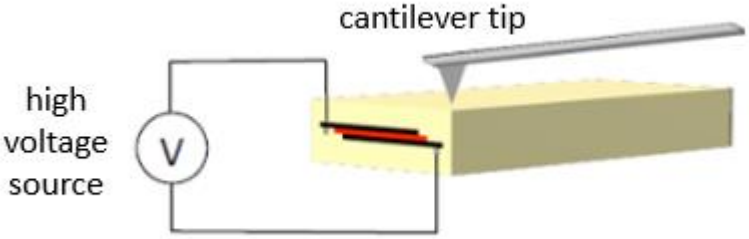

Figure 10. Schematic of experimental setup used for HVAFM measurements.

The fiber sample is affixed in epoxy on one face to a glass slide and connected to an external DC high voltage power source and placed under an AFM tip in tapping mode. Figure 11 shows the AFM tip displacement at the surface of the electrostrictive fiber as increasing voltage steps are applied to the fiber through the external power source. The observed tip displacement is consistent with electric field-induced contraction of the electrostrictive layer.

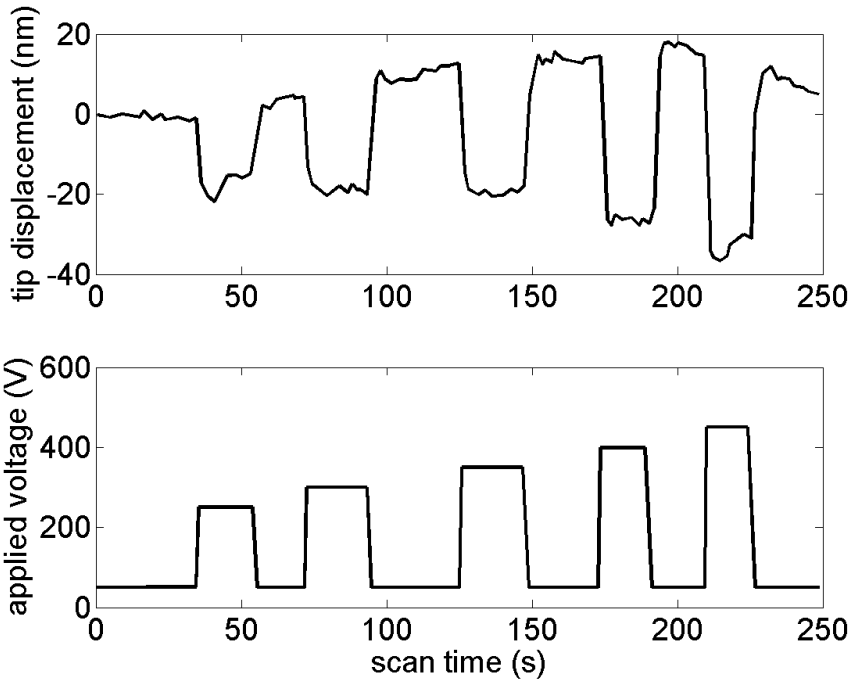

Figure 11. AFM cantilever tip displacement at the surface of the fiber under increasing voltage.

This measurement is repeated on different samples and the measured step heights are plotted against the applied voltage, both normalized by the average P(VDF-TrFE-CFE) layer thickness (figure 12).

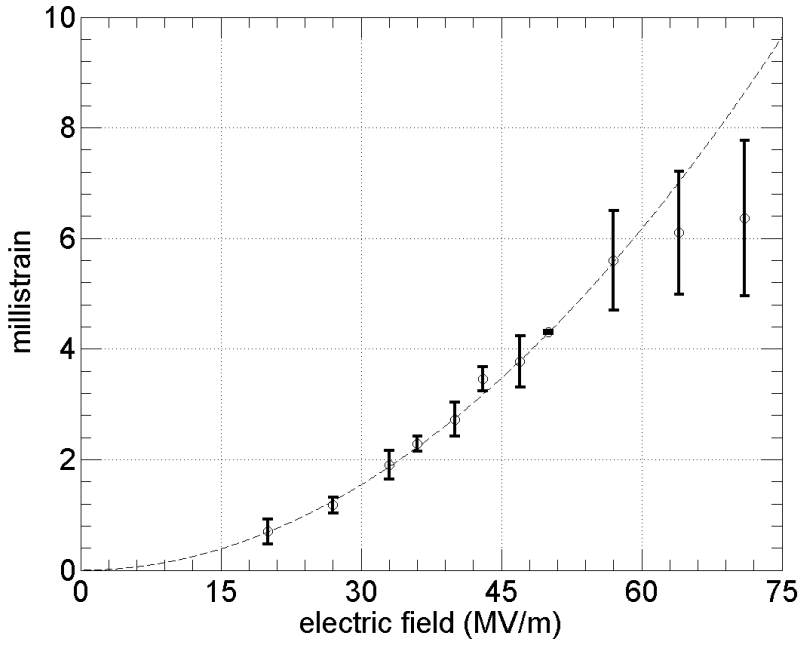

Figure 12. Measured electrostrictive strain as a function of the applied electric field in the terpolymer layer. The dotted line is a fit of the quadratic dependence between the strain and the electric field.

As expected, the electrostrictive strain shows a non-linear dependence on the electric field. Specifically, it follows a quadratic relation for low fields and tapers off at higher fields due to polarization saturation, as is typical for thickness strain plots for P(VDF-TrFE-CFE) [14,17]. The data spread at high fields is due to relaxation phenomena in the fiber, which result in different step heights when the voltage is turned on and off. A maximum strain of 0.78% is achieved for an applied electric field of 72 MV/m; this corresponded to a contraction of 52nm for a 7µm-thick terpolymer layer. This is considerably larger than strains achievable with piezoelectric

polymers, which are on the order of 0.1%. While higher values of longitudinal strain have been reported for free-standing P(VDF-TrFE-CFE) films [17], the electrostrictive layer in the fiber is constrained in the lateral direction by the PC cladding, therefore the amount of contraction it can undergo is limited by the Poisson effect. The experimental values obtained for the fibers match very well with literature values for field-induced longitudinal strains of P(VDF-TrFE-CFE) under clamped conditions [18]. We expect higher strain rates to be achievable by changing the fiber design such that the P(VDF-TrFE-CFE) layer would be constrained in the lateral direction by a softer material, for example low density polyethylene which has a Young's modulus one order of magnitude smaller than polycarbonate. The driving voltage required to achieve a given strain can also be lowered by adopting a stacked-layer geometry [6].

4.3 Contact Profilometry

The capability of the asymmetry in the strain field of the fiber to result in transverse deflection was investigated using contact profilometry. A schematic of the experimental setup is again shown in Figure 10, bearing resemblance to the HVAFM measurement setup but with cantilever tips designed for larger displacements; photographs of the setup are shown in Figure 13.

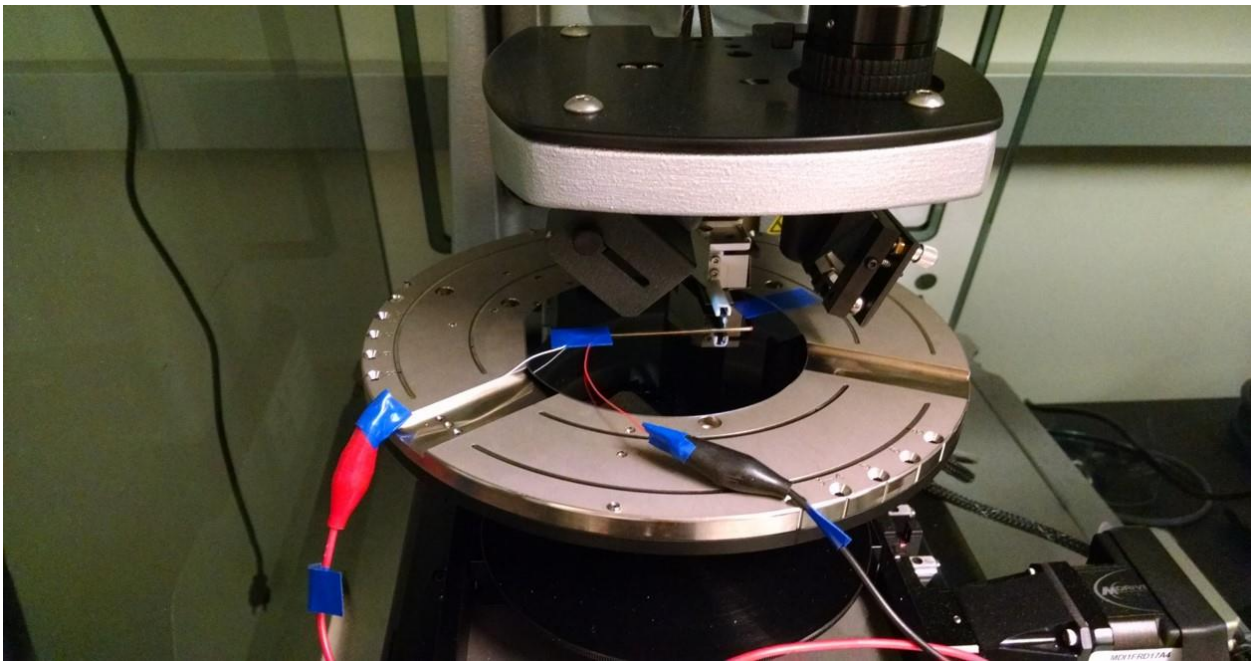

Figure 13. Photograph of a fiber sample on the stage of a contact profilometer, connected externally to a high voltage power supply.

For an applied voltage of 300VDC and contact force of 2mg, transverse deflection was measured along the axial direction of a 5cm fiber fixed flat on one end to a glass slide. The measurement was repeated for multiple fibers of the same length and the results shown in Figure 14. A maximum transverse displacement of 7µm is measured and the fiber is observed to bend toward the face containing the electrostrictive device. This asymmetry in the placement of the electrostrictive device is shown to be key in inducing a bending behavior that resembles a cantilever.

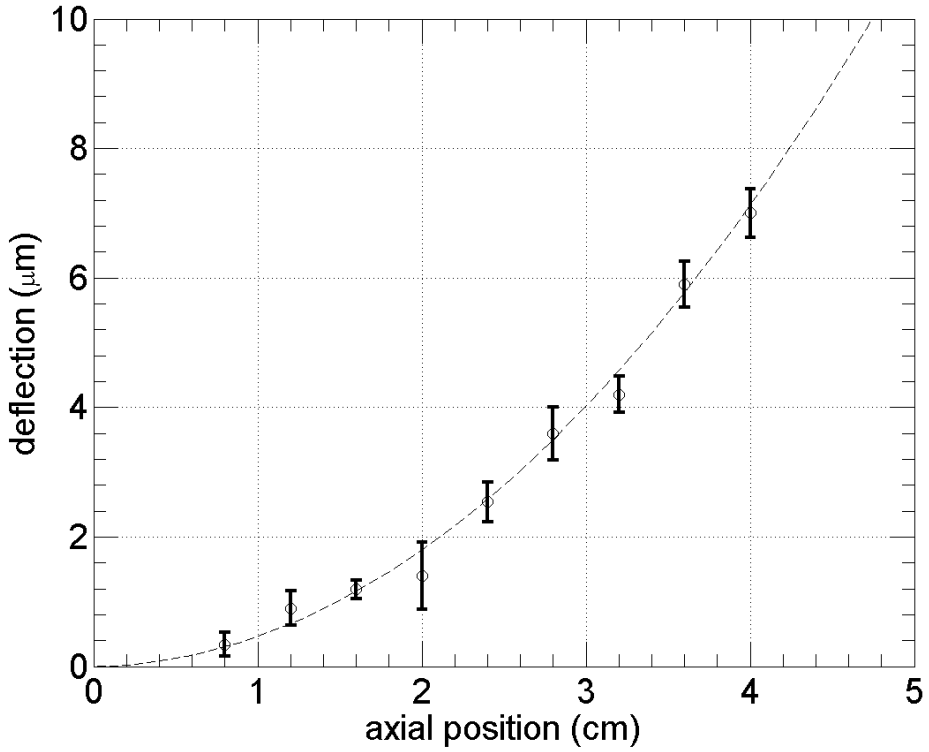

Figure 14. Contact profilometry measurement of fixed-end fiber deflection at 300V. The dotted line is a quadratic fit for the data.

Chapter 5

Fiber Actuation for Amplitude Modulation

In this chapter, having established that strain in the electrostrictive layer results in transverse deflection of the fiber, we illustrate the potential of our approach to construct MEMS in fibers by utilizing electrostrictive strain to perform amplitude modulation of an optical signal at harmonic frequencies of the fiber. We do this for both the single fiber case and for an array of fibers embedded in a polymer matrix.

5.1 Optical Setup

To measure modulation, a tunable laser is directed onto a face of the fiber that contains a mirror. The signal reflected back from the fiber surface is detected by a photodetector and recorded with an oscilloscope. The fiber is driven by an external high voltage power source and lock-in amplifier. A schematic of this setup is illustrated in Figure 15, and photographs are shown in Figure 16.

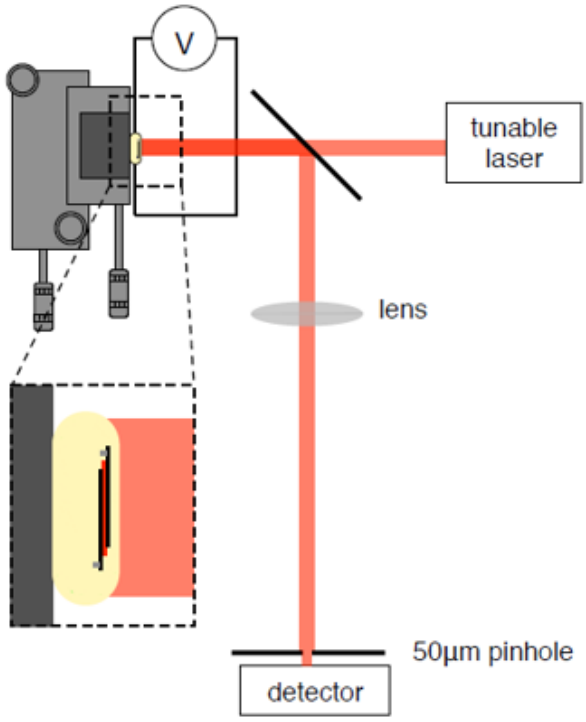

Figure 15. Optical set-up to measure amplitude modulation under applied voltage and driving frequency

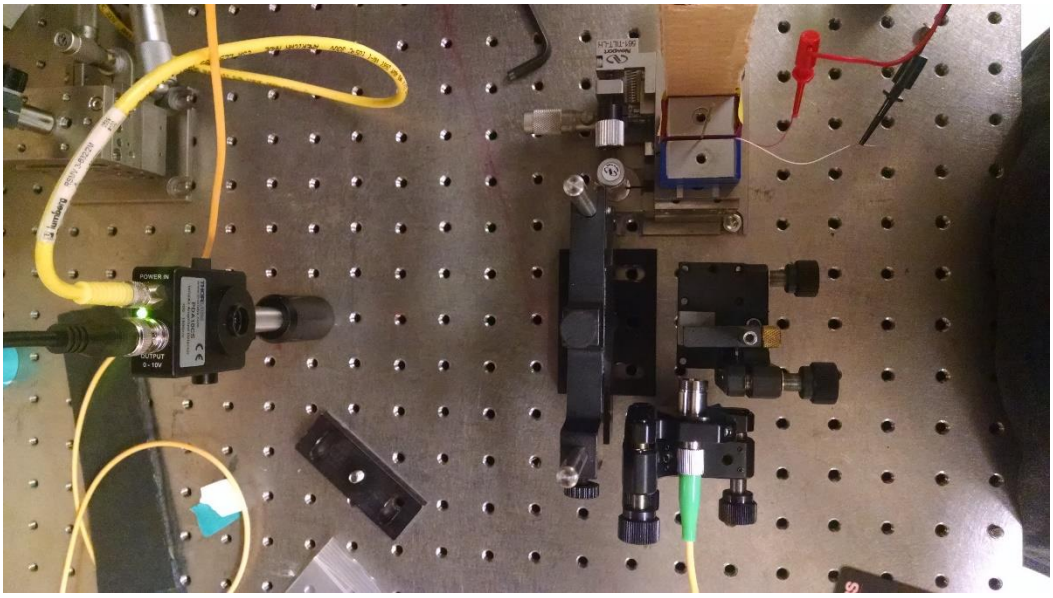

Figure 16. Photograph of optical setup used to measure amplitude modulation. The fiber is situated below the cardboard in the top of the image, the photodetector is the leftmost device, and the laser comes in from the bottom of the image through the fiber optic cable.

5.2 Amplitude Modulation Measurements

The measurement is performed by fixing the laser wavelength and recording the photodetector output with applied voltage. Modulation depth is calculated from the peak-to-peak voltage and the average voltage in the following manner:

$$\%MD = \frac{1}{2}\frac{V_{pp}}{V_{avg}} * 100 \quad (5)$$

This results in a maximum modulation depth of 22.5% at the first harmonic with an applied voltage of 90V, and 2.5% at the second harmonic with an applied voltage of 150V (figure 17).

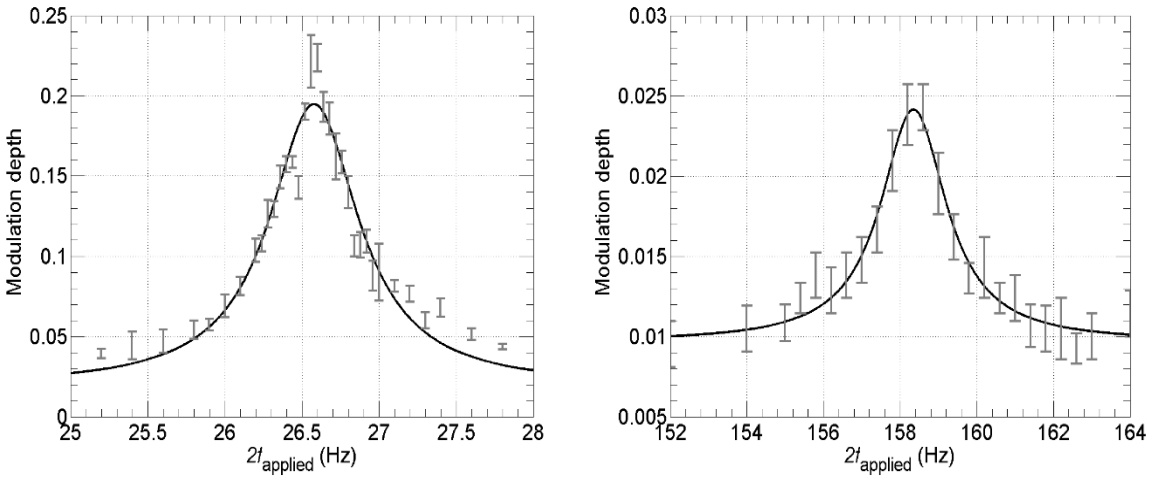

(a) (b)

Figure 17. a) Modulation depth measured in the vicinity of the first harmonic, approximately 26.6Hz. Solid line is a fitted Lorentzian curve. **b)** Modulation depth measured in the vicinity of the second harmonic, approximately 158.3Hz. Solid line is a fitted Lorentzian curve.

Prior to measurement, the first and second harmonic frequencies were predicted using solutions from the well-known Euler-Bernoulli beam theory:

$$\omega_i = \frac{x_i}{L^2}\sqrt{\frac{EI}{\lambda}} \quad (6)$$

where ω_i is the i-th resonance frequency, L is the length of the fiber, E is Young's modulus (2.0-2.6 GPa), I is the second area moment, λ is the mass per length ($1.2*10^3$ kg/m^3 * cross-section area in m^2), and x_i are known terms that depend on the boundary conditions of the problem.

At measured frequencies of 26.6Hz and 158.3Hz, respectively, they are shown to fall within the predicted ranges of 24.3±2Hz and 152±10Hz, respectively. A range of values in the predicted harmonic frequencies is reported due to uncertainty in the Young's modulus of the composite fibers as well as non-idealities in the fabricated fiber device. Additional work is in progress to model the impact of these factors.

5.3 Fiber Array in Polymer Matrix

Electrostrictive fibers embedded in a polymer matrix have the potential to form the functional unit of large surface area devices such as interactive haptic displays, acoustic modulators, and energy harvesting systems. We illustrate this potential by embedding fibers in a polydimethylsiloxane (PDMS) matrix and using the resulting composite (figure 18) to perform amplitude modulation of an optical signal at low frequencies.

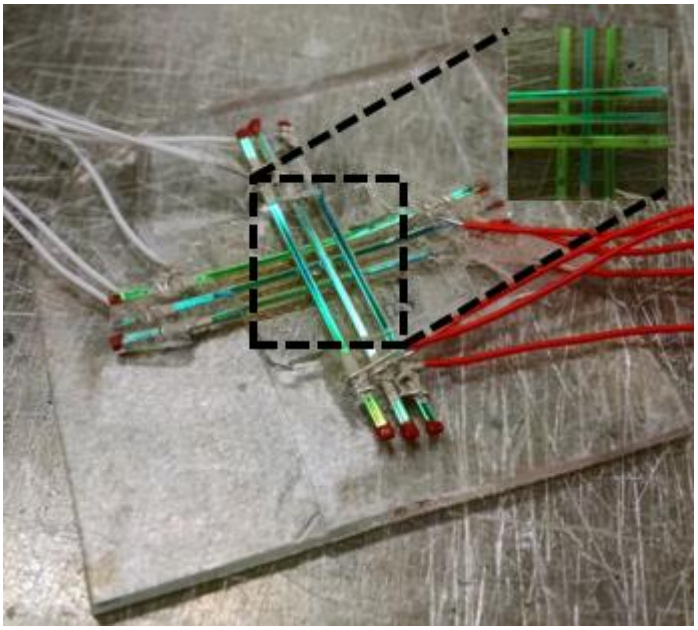

Figure 18. Fiber array embedded in PDMS, with inset showing close-up of location where fibers cross.

Modulation is measured using the previously described single fiber setup, and incident light is focused on the center of the fiber array. The output of the photodetector over time for a driving frequency of 1Hz and an applied voltage of 300V is shown in the lower half of Figure 19. The top half is an illustration of the relationship between driving frequency and fiber response frequency for an electrostrictive material, showing a characteristic frequency-doubling effect that can distinguish electrostriction from other forms of electromechanical transduction, such as piezoelectricity [9].

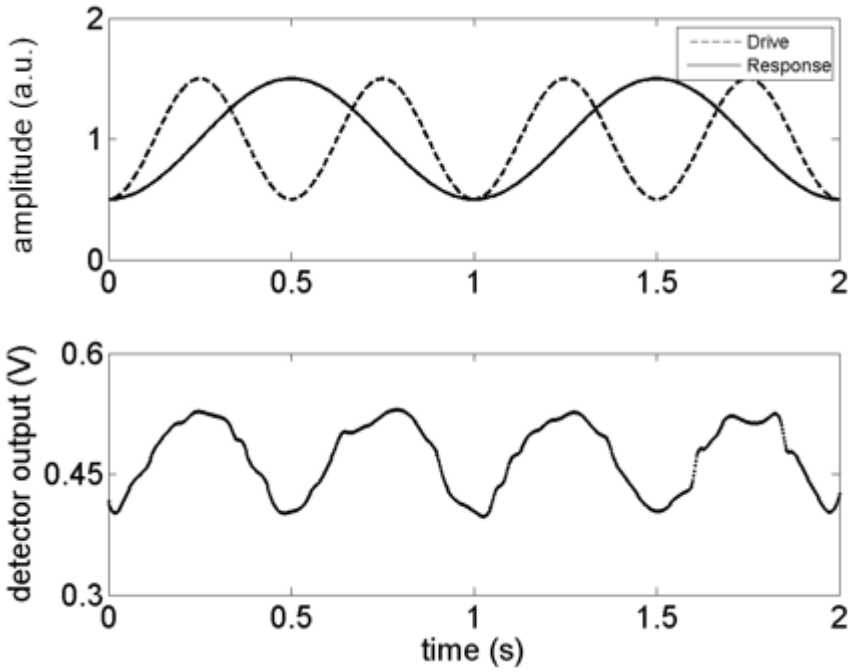

Figure 19. Top: illustration of characteristic frequency-doubling effect from electrostriction. A driving frequency of 1Hz results in a response frequency of 2Hz. Bottom: modulation of incident optical signal on a fiber array embedded in PDMS. Applied voltage is 300V at a driving frequency of 1Hz. Modulation depth is 25.8% for a fiber-to-sensor distance of 40cm.

Chapter 6

Conclusions and Future Directions

We have demonstrated the first integration of a relaxor ferroelectric polymer in a thermally drawn fiber for electromechanical actuation. Strains up to 0.78% were measured in the fiber device, resulting in a maximum transverse deflection of 7μm under an applied DC voltage of 300V. The potential of this approach to realize complex electromechanical systems in fibers is illustrated by the fabrication of an electrostrictive device capable of modulating a light source reflected off the surface of the fiber. Amplitude modulation of incident light through electric field induced deflection is demonstrated up to the second harmonic frequency of the fiber at 158.3Hz, and a modulation depth of 22.5% is reported; for an array of such fibers in PDMS, amplitude modulation is demonstrated at low frequencies with a modulation depth of 25.8%. If it is the case, a larger depth of modulation and a more uniform effect could be achieved by optimizing the fiber architecture, the fiber-to-sensor distance, and the reflectivity of the fiber surface.

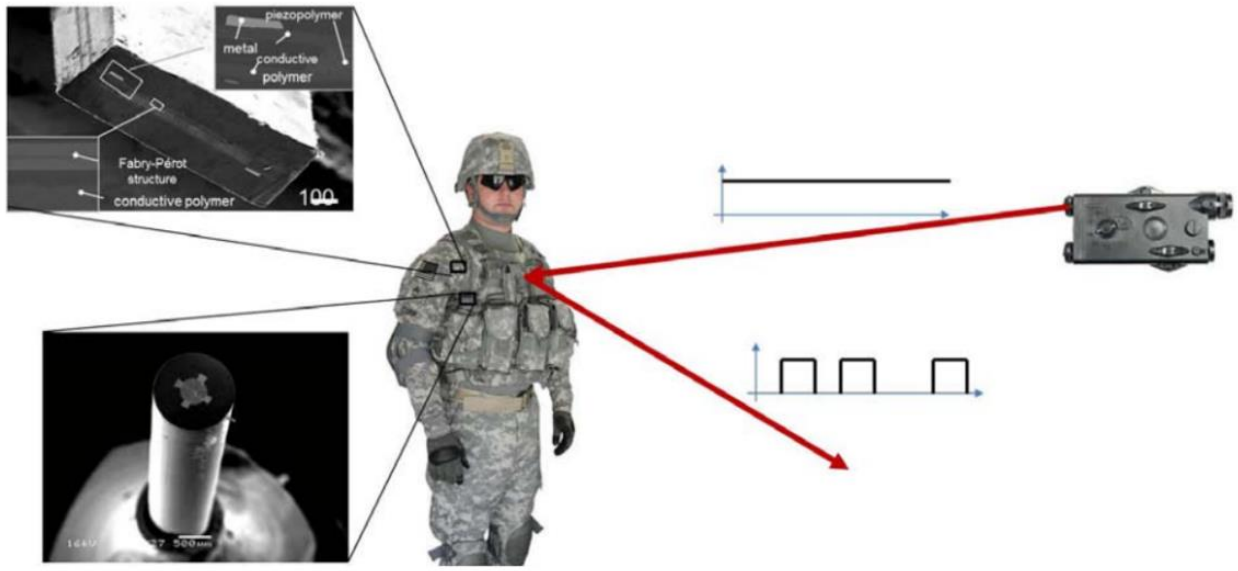

Figure 20. An embedded Fabry-Perot etalon can modulate reflected eye-safe laser beams by tuning the resonance of the etalon using a piezo transducer (courtesy of Dr. Ayman Abouraddy).

The integration of highly electrostrictive polymers in multimaterial fibers paves the way to the realization of sophisticated MEMS in fibers. Potential large surface-area applications include interactive haptic displays such as tactile Braille readers [22], color displays using tunable Fabry-Perot filters as pixel elements [23], and energy harvesting systems [24,25]. Photodiode fibers (receiver) and acousto-optic fibers (transmitter) in soldiers' uniforms can provide covert communication and IFF abilities [5], where an embedded Fabry-Perot etalon can modulate reflected eye-safe laser beams by tuning the resonance of the etalon using a piezo transducer (figure 20). Further applications could be enabled by integrating electrostrictive polymer devices with microfluidic channels in fibers [26], for example electrically controllable microfluidic pump [27] or liquid-filled varifocal lenses [28].

References

[1] R. P. Feynman, *Engineering and Science* **1960**, *23*, 22–36.

[2] K. Petersen, *Proceedings of the IEEE* **1982**, *70*, 420–457.

[3] C. Liu, *Foundations of MEMS (Second Edition)*, Prentice Hall, Upper Saddle River, NJ, **2012**.

[4] A. F. Abouraddy, M. Bayindir, G. Benoit, S. D. Hart, K. Kuriki, N. Orf, O. Shapira, F. Sorin, B. Temelkuran, Y. Fink, *Nat. Mater.* **2007**, *6*, 336–347.

[5] A. Abouraddy, O. Shapira, M. Bayindir, J. Arnold, F. Sorin, D. Hinczewski, J. Joannopoulos, Y. Fink, *Nat. Mater.* **2006**, *5*, 532–536.

[6] N. Chocat, G. Lestoquoy, Z. Wang, D. M. Rodgers, J. D. Joannopoulos, Y. Fink, *Advanced Materials* **2012**, n/a–n/a.

[7] M. Bayindir, F. Sorin, A. Abouraddy, J. Viens, S. Hart, J. Joannopoulos, Y. Fink, *Nature* **2004**, *431*, 826–829.

[8] S. Egusa, Z. Wang, N. Chocat, Z. M. Ruff, A. M. Stolyarov, D. Shemuly, F. Sorin, P. T. Rakich, J. D. Joannopoulos, Y. Fink, *Nat. Mater.* **2010**, *9*, 643–648.

[9] L. E. Cross, S. J. Jang, R. E. Newnham, S. Nomura, K. Uchino, *Ferroelectrics* **1980**, *23*, 187–191.

[10] J. Chen, A. Shurland, J. Perry, B. Ossmann, T. R. Gururaja, In *, Proceedings of the Tenth IEEE International Symposium on Applications of Ferroelectrics, 1996. ISAF '96*; 1996; Vol. 1, pp. 27 –30 vol.1.

[11] Newnham, R. E., Sundar, V., Yimnirun, R., Su, J. & Zhang, Q.M. Electrostriction: nonlinear electromechanical coupling in solid dielectrics. *The Journal of Physical Chemistry B* 101, 10141–10150 (1997).

[11] G. A. Smolensky, A. I. Agranovska, *Sov. Phys. Solid State* **1959**, *1*, 1429–1437.

[12] Q. M. Zhang, V. Bharti, X. Zhao, *Science* **1998**, *280*, 2101 –2104.

[13] H. S. Xu, Z. Y. Cheng, D. Olson, T. Mai, Q. M. Zhang, G. J. Kavarnos, *Applied Physics Letters* **2001**, *78*, 2360–2362.

[14] F. Xia, Z. -Y Cheng, H. S. Xu, H. F. Li, Q. M. Zhang, G. J. Kavarnos, R. Y. Ting, G. Abdul-Sadek, K. D. Belfield, *Advanced Materials* **2002**, *14*, 1574–1577.

[15] F. Bauer, *Applied Physics A: Materials Science & Processing* **2012**, *107*, 567–573.

[16] A. . Agronin, Y. Rosenwaks, R. G.I, *Nano Letters* **2003**, *3*, 169–171.

[17] F. Bauer, E. Fousson, Q. M. Zhang, *IEEE Transactions on Dielectrics and Electrical Insulation* **2006**, *13*, 1149–1154.

[18] D.-Y. Jeong, Y.-H. Ye, Q. M. Zhang, *Applied Physics Letters* **2004**, *85*, 4857–4859.

[19] G. Benoit, S. D. Hart, B. Temelkuran, J. D. Joannopoulos, Y. Fink, *Advanced Materials* **2003**, *15*, 2053.

[20] J. D. Joannopoulos, S. G. Johnson, J. N. Winn, R. D. Meade, *Photonic Crystals: Molding the Flow of Light (Second Edition)*, Princeton University Press, **2008**.

[21] Z. Ruff, D. Shemuly, X. Peng, O. Shapira, Z. Wang, Y. Fink, *Opt. Express* **2010**, *18*, 15697–15703.

[22] K. Ren, S. Liu, M. Lin, Y. Wang, Q. M. Zhang, *Sensors and Actuators A* **2008**, *143*, 335.

[23] Z. Sun, Q. Lin, *IEEE Photonics Technology Letters* **2008**, *20*, 1157–1159.

[24] H. Zhu, S. Pruvost, P. J. Cottinet, D. Guyomar, *Applied Physics Letters* **2011**, *98*, 222901–222901–3.

[25] M. Lallart, P.-J. Cottinet, D. Guyomar, L. Lebrun, *Journal of Polymer Science Part B: Polymer Physics* **2012**, *50*, 523–535.

[26] A. M. Stolyarov, L. Wei, O. Shapira, F. Sorin, S. L. Chua, J. D. Joannopoulos, Y. Fink, *Nature Photonics* **2012**, *6*, 229–233.

[27] F. Xia, S. Tadigadapa, Q. M. Zhang, *Sensors and Actuators A* **2006**, *125*, 346–352.

[28] S. T. Choi, J. Y. Lee, J. O. Kwon, S. Lee, W. Kim, *Liquid-filled varifocal lens on a chip*, **2009**.